Contributed paper

OPTO-ELECTRONICS REVIEW **11**(2), 99–111 (2003)

HgCdTe epilayers on GaAs: growth and devices

V.S. VARAVIN, V.V. VASILIEV, S.A. DVORETSKY*, N.N. MIKHAILOV, V.N. OVSYUK, YU.G. SIDOROV, A.O. SUSLYAKOV, M.V. YAKUSHEV, and A.L. ASEEV

Institute of Semiconductor Physics SB RAS, 13 Lavrentieva Av., 630090 Novosibirsk, Russia

View of basic and specific physical and chemical features of growth and defect formation in mercury cadmium telluride (MCT) heterostructures (HS's) on GaAs substrates by molecular beam epitaxy (MBE) was made. On the basis of this knowledge a new generation of ultra high vacuum set, ultra-fast ellipsometer of high accuracy and automatic system for control of technological processes was produced for reproducibility of growth MCT Hs's on substrates up to 4" in diameter. The development of industrially oriented technology of MCT HS's growth by MBE on GaAs substrates 2" in diameter and without intentional doping is presented. The electrical characteristics of n-type and p-type of MCT HS's and uniformity of MCT composition over the surface area are excellent. The residual donor and acceptor centres are supposed as hypothetically tellurium atoms in metallic sublattice ("antisite" tellurium) and double-ionised mercury vacancies. The technology of fabricating focal plane arrays is developed. The high quality characteristics of infrared detectors conductance and diode mode are measured. Calculations of detector parameters predicted the improvement in serial resistance and detectivity of infrared diode detectors based on MCT heterostructures with graded composition throughout the thickness.

Keywords: MCT, MBE, growth GaAs, Si, ellipsometer, heterostructures, infrared detectors, photoconductors, photodiodes, focal plane arrays, p-n junctions.

1. Introduction

$Cd_xHg_{1-x}Te$ (MCT) solid solution is the basic material for infrared detectors (IRD) that operate in a wide wavelength range (from 1 to 20 μm and over). The lattice constant of MCT is weekly changed for different compositions between CdTe and HgTe. This is very important for using complex MCT heterostructutres (HS's) for a new generation of IRD. Using different physical processes enables us to design different types of IRD operating in a wide temperature range (from liquid nitrogen temperature to room one).

The future development of multielement IRD needs increase in substrate dimension and uniformity of physical properties over the surface area. Now the basic research is focused on the growth, doping and characterization of MCT on lattice matched CdZnTe substrates because the highest crystal perfection is realized just for this material conjugation. CdZnTe substrates of a large area (up to 40×60 mm^2) are available and used for MCT growth. But the crystal perfection and Zn content are not uniform over the surface area [1]. Additionally, the disadvantages of CdZnTe substrates are high cost, absence of precise impurity control at growth, essential difference of coefficient of thermal expansion from silicon ones and low mechanical strength.

The alternative substrates (epilayers of CdTe or CdZnTe on Al_2O_3, GaAs, Si substrate, etc.) have the advantages in comparison with CdZnTe substrates from the point of view of substrate dimension, low cost and coefficients of thermal expansion are practically equal to the parameters of silicon which is used for production of read-out circuits. The most attractive from alternative substrates are those based on GaAs [2–4] and Si [5–7]. The disadvantages of such substrates are the large lattice mismatch of conjugation materials which is equal to ~14.6% for CdTe/GaAs and ~19% for CdTe/Si at room temperatures. This leads to decrease of MCT crystalline perfection in comparison with the use of CdZnTe substrates. The MCT quality on GaAs must be better than that for MCT on Si. The advantage of using Si substrates for growth of MCT HS's is the possibility of creating photosensitive MCT epilayer and read-out circuit in monolithic hybridisation scheme.

The most attractive method for growing MCT epitaxial material is MBE technique because of its flexibility, simplicity and many advantages over the others techniques. There is demonstrated the fabrication of SWIR [8], MWIR [9], LWIR [10] and VLWIR [11] detectors on the basis of MCT HS's grown on CdZnTe, GaAs by MBE with the photoelectrical characteristics compared with analogous ones for IRD on basis of MCT epilayers grown by LPE and MOVPE. From MCT HS's MBE on Si only MWIR devices with high quality characteristics were fabricated now. The parameters of IRD depend on crystalline perfection of

*e-mail: dvor@isp.nsc.ru

MCT material. The dislocation density (Nd) essentially influences on parameters of LWIR diodes detectors [12,13] which operated at low temperatures. The calculation showed that for LWIR region R_0A product at 77 K was strongly dependent on dislocation densities over 10^6 cm^{-2} [14]. The dislocation density of MCT HS's on GaAs substrate after the growth is at level near 10^6 cm^{-2} and over and decrease up to 2×10^5 cm^{-2} after annealing at elevated temperatures [15]. This means that it is possible to grow MCT HS's on GaAs which is suitable for fabricating diode type IRD. Earlier, it was shown that the minority carrier lifetime τ of n-type MCT HS's on GaAs substrates without widegap layer at boundaries was 220 ns at minimal dislocation density and decrease up to few tens with increasing dislocation density. We showed that the minority lifetime at dislocation density 5×10^7 cm^{-2} is close to 1000 ns for MCT HS's on GaAs with a widegap layer at film boundaries [16]. These values are two orders higher than for MCT HS's on GaAs without a wide gap layer. So, MCT HS's with widegap layer may be used for fabricating photoconductors.

The important parameter at fabricating photovoltaic IRD is minority carrier lifetime. The minority carrier lifetime determines the diffusion length and dark current of a diode. MCT bulk crystal or epilayers of p-type conductivity for photovoltaic IRD are fabricated by thermal annealing of as-grown material. The minority lifetime of LWIR MCT is up to 10–20 nanoseconds and is limited by double ionised mercury vacancies [17,18]. The values of diffusion length (optical area of diode) of minority carriers (electron in *p*-type MCT) for $\tau = 10$ ns and different mobilities are presented in Table 1.

Table 1. The values of diffusion length of electron in *p*-type MCT.

τ (ns)	μ (cm^2/Vs)	L (μm)
10	10000	8.0
10	50000	17,9
10	100000	25.3

It can be seen that *p*-type MCT material may be used for production of photovoltaic focal plane arrays which pixel dimensions and pitches are compared with diffusion length. The modern tendencies are decreasing the FPA's pixel dimensions and pitches and increasing number of elements. So, p-type MCT HS's MBE fabricating by annealing are suitable for production of FPA's with small pixel dimensions and pitches. It is necessary to remark that for such FPA's one can eliminate cross talking between neighbouring diodes.

The purpose of this paper is the overview of progress on development of industrially oriented equipment, control technique and technology of growth process of MCT HS's by MBE on GaAs substrates, technology of fabricating focal plane arrays and characteristics of infrared photoconductors and photodiodes.

2. Epilayers growth

2.1. Basic features of MCT growth by MBE

MBE is a developed and widely used epitaxial method for growth of narrow-gap mercury content A^2B^6 HS's and, first of all, for growth of MCT on CdZnTe and alternative substrates. The status of MCT MBE technology has reached the level for producing material used for industrial production of high quality IR devices.

MBE offers many advantages over other epitaxial methods of MCT growth due to several reasons:

- MCT film growth is carried out at lowest temperatures (160°C–200°C) as compared with 450°C for LPE and 250°C–400°C for MOVPE. The reduction of growth temperature precludes impurity diffusion from the substrate into MCT films resulting in reduction of the background doping down to 1–1.5 order at the same purity of material for MCT synthesis,
- unlike in LPE, no aggressive medium is present in MBE that leads to use of alternative substrates,
- the control of growth and MCT films parameters *in situ* gives possibility to fabricate structures with desired MCT composition distribution throughout the thickness for a multicolour IRD. The control of MCT composition *in situ* allows to grow heterojunctions of top quality,
- MBE is an ideal technique for growing CdTe/HgTe superlattices and other nanostructures.

The detailed investigations of physical and chemical foundations of growth process, mechanism of defect formation, nature of residual doping for realisation of evident MBE advantages were carried out. It was found that there exist the fundamental physical and chemical reasons that determine MCT film quality at growth by MBE. These reasons are as follows:

- relationship between equivalent beam pressures (EBP) of mercury and tellurium ($P_{(ebpHg)}/P_{(ebpTe2)}$),
- growth temperature,
- substrate orientation,
- nature of tellurium in molecular flux.

At a fixed substrate temperature and growth rate the interval of optimal $P_{(ebp\ Hg)}/P_{(ebp\ Te2)}$ is needed for MCT film growth with minimal defect densities, excellent electrical parameters [19]. At the fixed value of $P_{(ebp\ Hg)}/P_{(ebp\ Te2)}$ and growth rate there exists an interval of optimal temperatures for growth of crystalline perfection MCT films [19]. At deviation of $P_{(ebp\ Hg)}/P_{(ebp\ Te2)}$ and temperatures from optimal ones a sharp decrease in MCT film crystalline quality (increase in densities of surface defects, microtwins in volume, etc.), poor electrical parameters is observed. The quality of MCT films depends on substrate orientation. It was shown that the highest MCT film quality was reached at growth on vicinal substrate orientation even at high growth rates (up to 7–10 μm/h). The (112) substrate orientation is mainly used for growth of MCT films. However, the range of growth conditions ($P_{(ebp\ Hg)}/P_{(ebp\ Te2)}$ and temperatures) is enough narrow for growth of high quality

MCT films. We found that the range of growth conditions may be extended without decreasing MCT film quality at growth on (013) substrates.

The important reason of defect formation during MCT growth by MBE is the nature of tellurium which exists mainly as diatomic molecules in a molecular flux. On a growth surface, diatomic tellurium molecules reacted with mercury and cadmium atoms with the crystallization of MCT compound by the following reactions:

- dissociation of diatomic tellurium molecules onto atoms
  $Te_{2\ (ads)} \rightarrow 2\ Te_{\ (ads)}$,
- crystallisation of mercury cadmium telluride compounds
  $Cd_{\ (ads)} + Te_{\ (ads)} \rightarrow CdTe_{\ (s)}$,
  $Hg_{\ (ads)} + Te_{\ (ads)} \rightarrow HgTe_{\ (s)}$.

Kinetic limitations of reactions at low temperatures of MCT compound crystallisation lead to formation of tellurium segregations and substitution of cadmium and mercury in metallic crystal sublattice by the following reaction:

- deposition of tellurium in solid phase
  $Te_{2\ (ads)} \rightarrow Te_{2\ (s)}$,
- incorporation of diatomic molecules into crystal lattice
  $Te_{2\ (ads.)} \rightarrow Te_{(m)}$-Te.

In the first case, tellurium deposition in a solid phase is a reason of V-defects (voids) formation. In the second case, tellurium on metallic site ($Te_{(m)}$ so-called "antisite" tellurium) is a probable residual donor centre for MCT films growth by MBE.

The scheme of crystallisation processes of MCT films with diatomic tellurium molecules is shown in Fig. 1.

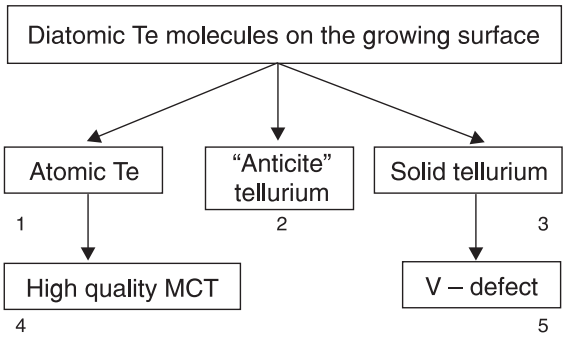

Fig. 1. The scheme of crystallization processes of MCT films by MBE: 1 – dissociation of diatomic Te molecules on atoms, 2 – incorporation of diatomic Te molecules in MCT crystal lattice, 3 – deposition of diatomic Te molecules in solid phase, 4 – reactions of Te atoms with cadmium and mercury for high quality MCT growth, 5 – formation of V-defects (voids).

The development and production of efficient equipment, control technique of growth processes *in situ*, the growth technology (including MCT growth on large in dimension GaAs and Si substrates) allows all advantages of MBE to be realised and used in future for industrial MCT production.

2.2. Specific features at MCT growth on GaAs

Specific features of MCT deposition on GaAs substrate are the basic features at deposition of CdZnTe layers on GaAs. The deposition of MCT films on GaAs substrate without a buffer layer at low temperatures did not allow the material of required quality for device application to grow. The essential success has been reached in MCT film growth on "alternative" substrates – CdZnTe buffer layer on GaAs substrate. The growth of ZnTe, CdTe or its compounds on GaAs of good quality is connected with specific features of defect formation at conjugation of II–VI and III–V compounds:

- nonisovalency of conjugation of CdZnTe and GaAs substrates,
- large mismatch between CdZnTe and GaAs,
- doping of MCT by gallium from GaAs substrate.

At conjugation of A^2B^6 and A^3B^5, Si the excess of valence electrons leads to distortion of tetrahedral configuration of a compound on the interface (formation of two or three atomic bonds instead of four ones) and as a consequence to change a layer orientation from a substrate one. Chemical interaction on A^2B^6/GaAs interface at the initial growth stage plays a critical role in formation of surface morphology and structural defects. The main reason for that is the change of average value of valence electrons at the interface upon substitution of As by Te and formation of Ga-Te bonds in a crystal lattice. The tendency to eliminate the excess of valence electrons at the interface leads to formation of facets, twins and change of stoichiometry of growth structure.

A large mismatch of CdZnTe and GaAs is responsible for disordered phase, dislocations and orientation mixture of grown film [20,21]. It was found that the growth temperatures, molecular flux intensities, substrate orientations influenced on facets formation, twinning, stochiometric breaking and formation of disordered phase at the initial stage of CdTe growth on GaAs substrate. The following technological operations allow dividing these problems as:

- use of vicinal GaAs surface for creation of a system of regular nuclei growth centres,
- control of compound formation and nucleation at the initial stage of growth,
- growth of ZnTe film on atomic clean GaAs surface to prevent the appearance of the mixture of orientation,
- growth of CdTe films on ZnTe/GaAs surface with the thickness 5–7 μm,
- accurate control of optimal molecular fluxes and their relationships and substrate temperatures.

The auto doping of MCT film at growth on CdZnTe/GaAs substrates by MBE was suggested by SIMS analysis. However, electrical parameters show no correlation with Ga content in MCT film volume. In fact, the Ga content into MCT film volume exceeds the observed electron concentration. It means that Ga is incorporated in a neutral position in a crystalline lattice. The thermodynamic calculation of equilibrium Ga concentration versus temperature

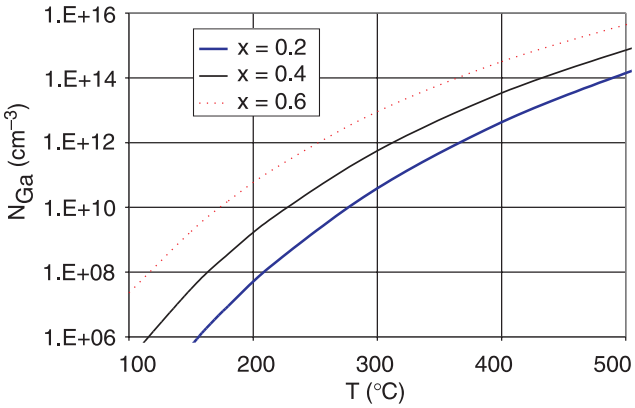

Fig. 2. Dependencies of equilibrium electrically active Ga concentration in MCT on temperature and composition.

dependence with the presence of Ga_2Te_3 taking into account was carried out [22]. In Fig. 2, the equilibrium concentration of electrically active Ga is shown.

It was found that Ga concentration sharply decreased with decreasing temperature and became lower than 10^8 cm^{-3} at temperatures below 200°C for MCT composition $X_{CdTe} = 0.2$. Annealing MCT films at the temperatures over 300°C can lead to increase in electron concentration because of transition of Ga atoms in an electrically active state. Really, electron concentration at 10^{17} cm^{-3} level was observed on annealing at 500°C.

Taking into account the basic and specific features of MCT growth on GaAs substrates the equipment and technology has been developed for CdZnTe buffer layer growth on GaAs substrate and following MCT films growth with minimal defect density by MBE method.

3. Industrially-oriented production of MCT epilayers

3.1. Equipment

Industrially oriented production is being developed for manufacturing trivial and novel type of MCT HS's MBE on (013)GaAs substrates 2" in diameter for different types of IRD.

MCT HS's MBE production is based on the following elements:

- new generation of ultra high vacuum multichamber set equipped with big-capacity molecular beam sources for growth on a substrates up to 4" in diameter with high composition uniformity over the surface area; precise built-in ultrafast ellipsometer (UFE) for control of film parameters *in situ* and an automatic system for control of technological processes,
- technological operating sequences for production of n-type and p-type MCT HS's with the parameters needed for qualitative photoconductors and photodiodes,
- equipment for characterization of MCT HS's parameters (composition, carriers concentration and their mobility, lifetime, density of surface defects, etc.).

Ultra high vacuum installation includes three technological chambers, two loading-unloading chambers and modules for transport racks and laminar dust free box.

A technological chamber for growth of buffer layer (BL) is equipped with ring-shaped Cd and Zn molecular beam sources which are mounted coaxially with a cylindrical type of tellurium molecular beam source and high-energy electron diffraction (HEED) system. A techno-

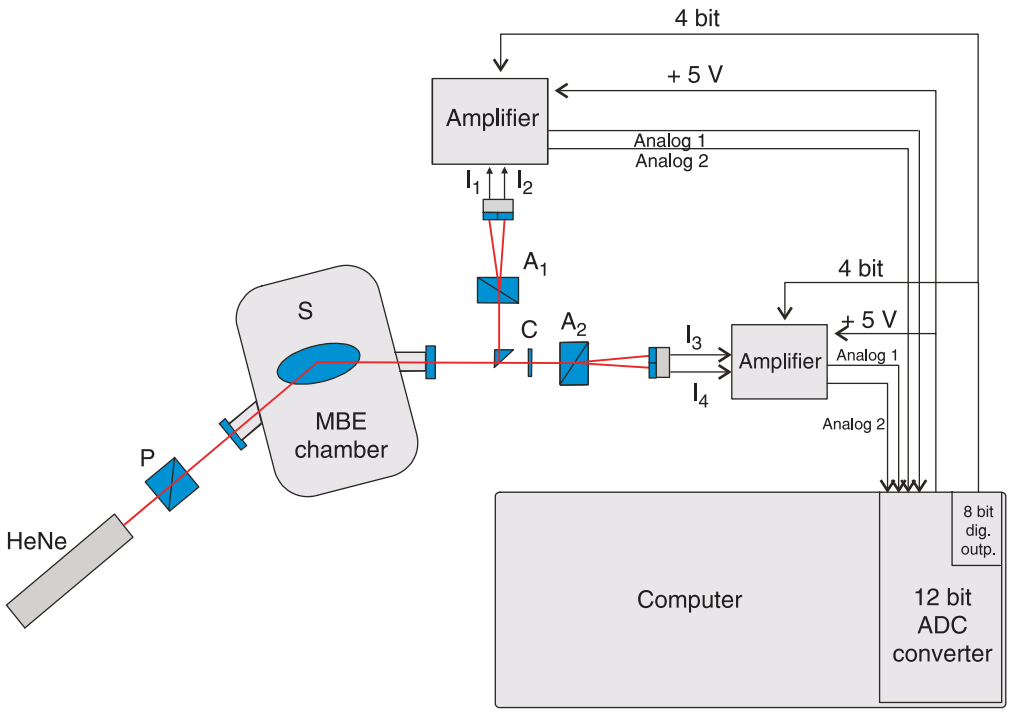

Fig. 3. Ultra-fast *in situ* operating ellipsometer LEF-751.

logical chamber for growth of MCT layer is equipped with ring-shaped Cd molecular beam source which is mounted coaxially with a cylindrical type of tellurium molecular beam source and built-in UFE system. Molecular beam sources provide high uniformity of fluxes over a large area at minimal consumption of evaporated high cost materials. The calculation showed that at accurate positioning of molecular beam sources MCT composition gradient over the surface area must be not worse than 0.0002 cm^{-1}. It is better by one order of magnitude than uniformity of MCT composition needed for multielement IRD.

Automatic (AE) types LEF–751 [23] and LEF–755 are remarkable due to their high speed and accuracy. They are used for measurement of growth rate, composition and surface morphology during MCT HS growth. MCT film composition X_{CdTe} is deduced from ellipsometric parameter Ψ being measured by UFE. Surface morphology is controlled by the ellipsometric parameter Δ. The ultra-fast ellipsometer (UFE) *in situ* LEF-751 is shown in Fig. 3.

To achieve the highest speed of measurement at high accuracy a new two-channel static ellipsometer system has been designed where two measuring channels (amplitude and phase) were spatially divided. The first channel (polariser–sample–analyser: PSA_1) is intended for Ψ measurement, the second one (polariser–sample–compensator–analyser: $PSCA_2$) is intended for measurement of Δ.

Laser beam, linearly polarised by the polariser P incidents onto the sample surface S. One part of the reflected beam is directed into the channel ψ by the total reflection prism R. The total reflection prism has no dichroism and does not include an error in ψ measurement. The second beam passes through the channel Δ without direction change. Both channels are designed identically, except the compensator C placed in channel Δ.

In either channel the light beam is splitted by a Wollaston prism employed as the analyser $A_1(A_2)$ into two orthogonally polarized beams. These beams strike photosensing areas of two-element photodiodes producing electrical signals I_1, I_2, I_3, and I_4. During measurement, the polarization elements are fixed at the azimuth position: polariser $P = 45°$, compensator $C = 45°$. The analyser A_2 has two fixed positions: 0° and 45° for complete polarization measurement. The ellipsometric parameters ψ and Δ are calculated from four signals using the following equations

$$\frac{I_1 - I_2}{I_1 + I_2} = \cos 2\psi, \qquad (1)$$

$$\frac{I_3 - I_4}{I_3 + I_4} = \sin 2\psi \sin \Delta, \quad \text{when} \quad A_2 = 0, \qquad (2)$$

$$\frac{I_3 - I_4}{I_3 + I_4} = \sin 2\psi \cos \Delta, \quad \text{when} \quad A_2 = 45, \qquad (3)$$

One more important advantage of the system is insensitivity to fluctuation of light intensity.

Absence of movable parts and signal modulation during measurement has provided very high speed limited only by amplifier-digitalizing capability.

The measurement time is mainly limited by digitisation. If digitisation time of ADC is 10 μs, the measurement of one pair of ψ and Δ from four electrical signals takes 40 μs. The speed of the ellipsometer is certainly not limited by these values. Potentially the ellipsometer system allows measurement with nanosecond and picosecond time resolution.

Ellipsometers have the following performance specification for MCT film measurement:

- absolute accuracy of film composition X_{CdTe} measurement ±0.005,
- sensitivity to composition X_{CdTe} variation ±0.0005,
- minimal film thickness to be measured 0.5 nm.

3.2. Technology

The technology of MCT HS's MBE production on (013)GaAs includes the following operations:

- chemical etching of GaAs substrate,
- thermal treatment of GaAs surface in arsenic flux in vacuum,
- growth of CdZnTe buffer layer on an atomic clean GaAs surface,
- growth of MCT on a buffer layer.

The high sensitivity and time resolution of UFE allows high-accuracy measuring of growth rate, thickness at growth of buffer and MCT layers, MCT composition and its changing under steady state growth condition. At growth of MCT film on CdTe, the ellipsometric parameters Δ and ψ in Δ-ψ plane is represented by a convergent spiral. The points on this curve at constant MCT correspond to film thickness. The final point of the spiral corresponds to definite MCT composition.

Dependencies of ellipsometric parameters Δ and ψ in Δ-ψ plane for initial growth stage are shown in Fig. 4(a) and at sharp changing of Te flux during MCT growth in Fig. 4(b).

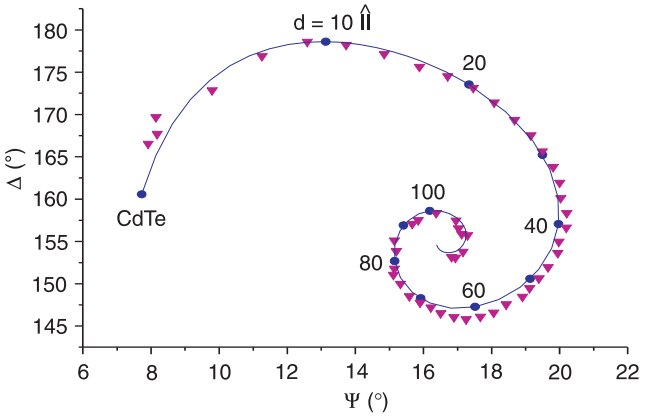

Fig. 4(a). The evolution of ellipsometric parameters at initial growth stage of MCT film (X_{CdTe} ~0.4) on CdTe. Dots – experiment; solid curve-calculation. Numbers on the curve correspond to film thickness in nm.

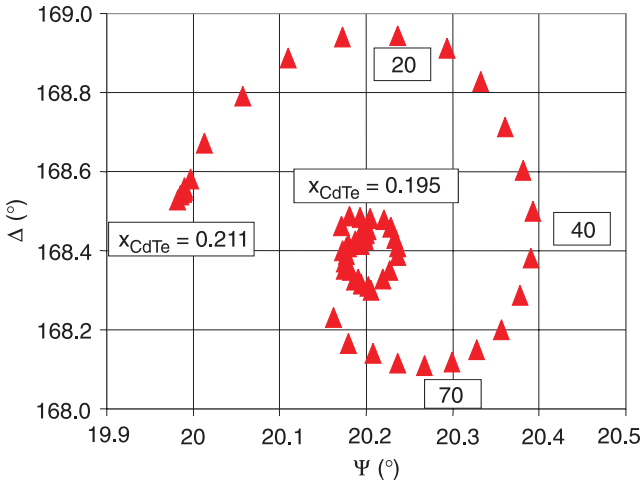

Fig. 4(b). The evolution of ellipsometric parameters at growth of MCT film (X_{CdTe} ~0.195) on MCT substrate (X_{CdTe} ~0.211). Numbers on the curve correspond to film thickness in nm.

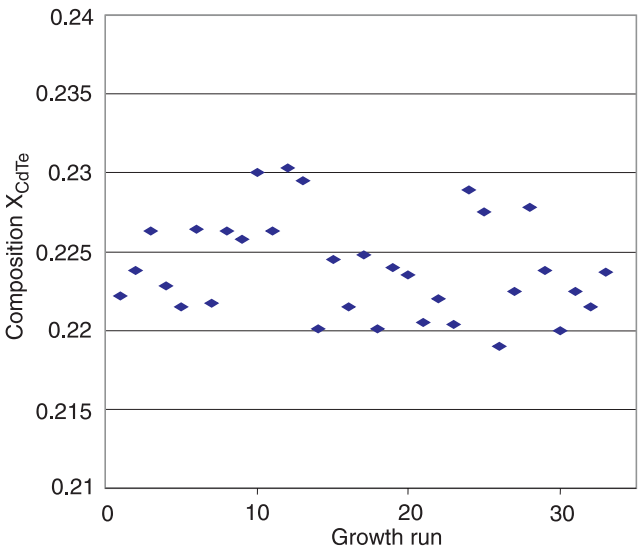

Fig. 5(a). The reproducibility of MCT composition at growth of MCT HS's MBE for LWIR photodiodes.

In Fig. 4(a), a convergent spiral represents the growth of MCT film with composition X_{CdTe} ~0.4 on CdTe. Large change of Δ and ψ, especially for MCT thickness up to 10 nm, demonstrates the possibility of growing nanostructures using UFE precise control. In Fig. 4(b), a convergent spiral demonstrates the sequence of MCT growth with a small change of composition. At growth of MCT film (X_{CdTe} ~0.211) tellurium flux was sharply increased. At convergent spiral corresponding growth of MCT film (X_{CdTe} ~0.195) was observed. It means that UFE control allows MCT layers to grow with precise measurement of thickness and composition for thick films as well as for superlattices. At the initial stage the growth rate is determined and used for subsequent determination of MCT thickness *in situ*.

UFE control may be used with success for reproducibility of MCT composition during growth run. In Fig. 5(a), the reproducibility of MCT composition is shown for growth run at production MCT HS's for LWIR photodiodes. The average mean X_{CdTe} = 0.224, standard deviation ΔX_{CdTe} = 0.0031 and $\Delta X_{CdTe}/X_{CdTe}$ = 1.4%. In the following growth series MCT composition was changed. In Fig. 5(b), the reproducibility of MCT composition is shown for growth run at production of MCT HS's for LWIR photoconductors. The average mean X_{CdTe} = 0.2137, standard deviation ΔX_{CdTe} = 0.002 and $\Delta X_{CdTe}/X_{CdTe}$ = 0.93%.

Technology of a novel type of MCT HS MBE with control over changing composition throughout the thickness was developed using UFE control. MCT HS's MBE with composition in an active layer X_{CdTe} = 0.20–0.35 and thickness 5–15 μm were grown without intentional doping [24]. Growth temperatures were 180–200°C and growth rate was 2–3 μm/h.

Electrical characteristics were determined from Hall measurements at 77 K by Van der Paw method. As grown MCT HS's MBE had n-type conductivity. Electron concentration and mobility were 10^{14}–10^{15} cm^{-3} and over 10^5 cm^2/Vs for composition X_{CdTe} ~ 0.20–0.22 and (8–50)×10^{13} cm^{-3} and (3–4)×10^4 cm^2/Vs for composition X_{CdTe} ~0.30–0.35, correspondingly. Carrier concentration was found to decrease with increasing growth temperature and MCT composition. The minority carrier lifetime was 2–10 μs for X_{CdTe} ~ 0.20–0.22 and 5–15 μsec for X_{CdTe} ~ 0.30–0.35. For conversion of as-grown n-type MCT HS's MBE to p-type annealing in helium atmosphere was carried out at 200–250°C and low mercury vapor pressure. After annealing, the hole concentration and mobility were (5–20)×10^{15} cm^{-3} and 400–700 cm^2/Vs for composition X_{CdTe} ~ 0.20–0.22 and (3–50)×10^{15} cm^{-3} and 300–500 cm^2/Vs for composition X_{CdTe} ~ 0.30–0.35, correspondingly.

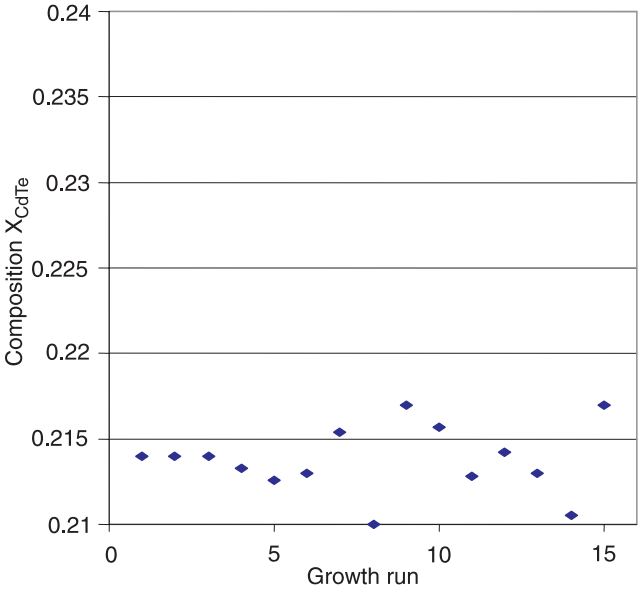

Fig. 5(b). The reproducibility of MCT composition at growth of MCT HS's MBE for LWIR photoconductors.

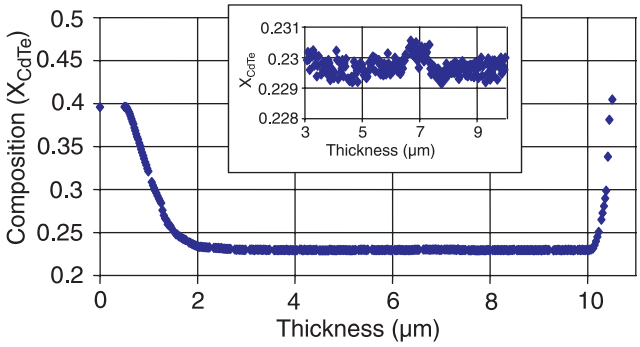

Fig. 6(a). MCT composition profile throughout the thickness with widegap layers at boundaries, measured by UFE *in situ*.

Experimental results of annealing and growth influence on electrical properties of MCT HS's MBE allow to suppose the presence of mobile acceptor centres and immobile donor centres. The most appropriate donor centres are anticite tellurium atoms [25].

The distribution of MCT composition throughout the thickness of a novel MCT HS's MBE was designed with the purpose to optimise IRD parameters. Figure 6 illustrates a novel MCT HS MBE with variation of MCT composition on boundaries of active layer. In Fig. 6(a), the MCT composition profile with widegap layers at the interface and at the surface is shown. Widegap layers created built-in electric fields in which non-equilibrium carriers drove back into the volume from surfaces with high recombination velocities and acted as passivating coatings [26,27]. Passivating widegap layers led to the essential increase in minority lifetime. In Fig. 6(b), MCT composition profile with narrowgap layer at the interface is shown. There is a "hillock" between narrowgap and active layers. Narrowgap layer sharply decreases diodes series resistance.

MCT composition, over 2" in sample diameter MBE HS's MCT, was measured across transmission spectra obtained by IR spectrometer (IKS-31) with sampling area of 20 mm^2 (Fig. 7). The best result shown that maximal changing of MCT composition along diameter did not exceed 0.001 that compared with calculated value. At industry production, the changing of MCT composition along diameter is not worse than 0.005.

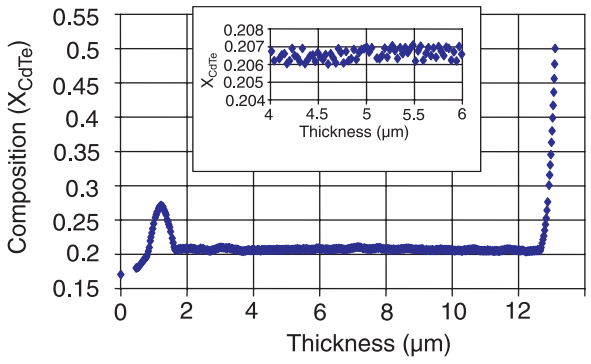

Fig. 6(b). MCT composition profile throughout the thickness with narrowgap layer at the interface, measured by UFE *in situ*.

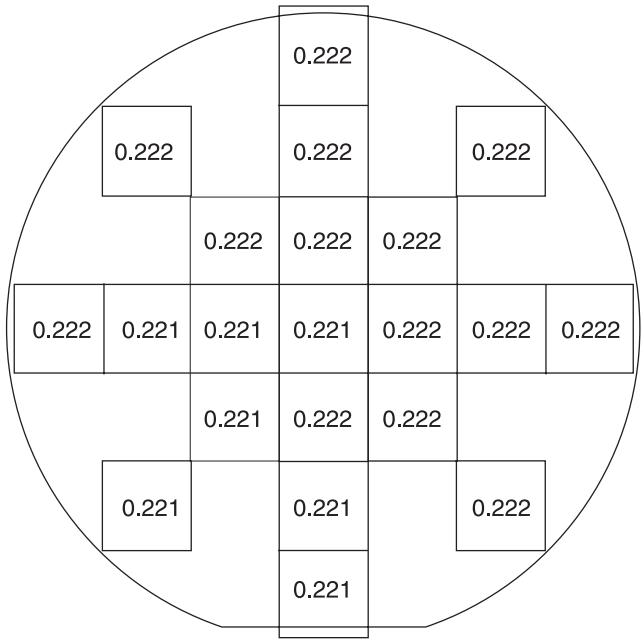

Fig. 7. MCT composition (X_{CdTe}) uniformity over surface area of MCT HS MBE on GaAs 2" in diameter.

4. Devices

4.1. Photoconductors

For manufacturing photoconductors (PC) cooled down to liquid nitrogen temperature, n-type HS's MCT MBE were used [28]. For manufacturing weakly cooled PC mainly p-type HS's MCT MBE were used. HS MCT MBE had widegap layers with variable composition at the interface and near the surface. Typical thickness of such a surface layer is 0.5–1 μm, with composition variation on the surface in relation to the active layer composition X_{CdTe} = +(0.15–0.3). The thickness of the active layer was 5–15 μm. The PC with areas from 0.1×0.1 mm up to 1×1 mm were manufactured by mesa technology using low temperature photolithography (T < 90°C). For side surfaces protection of the mesa structures, additional passivation was usually carried out. Native oxide and SiO_2, Si_3N_4, ZnS layers were used for passivation. ZnS layers were also used as antireflection coating.

Typical PC's characteristics (at 77 K) with the cut-off wavelength λ_c in 10–12 μm wavelength range or even shorter correspond to the published data of PC manufactured of bulk material and LPE films. In reality, PC's operates in the condition of background regime.

For a very long wavelength range PC (λ_c ~ 20 μm and over) the typical D^* value is near 5×10^{10} cmHz$^{1/2}$/W and achieves the values up to 2×10^{11} cmHz$^{1/2}$/W for the best PC's. Figure 8 (curve 1) presents spectral characteristic of PC with λ_c = 17.7 μm, sensitive area 0.1×0.1 mm and D^* (λ_{max},1 kHz,20°,1 Hz) = 1.7×10^{11} cmHz$^{1/2}$/W. Sharp long wave edge is indicative of high uniformity composition of operating layer of MCT HS MBE.

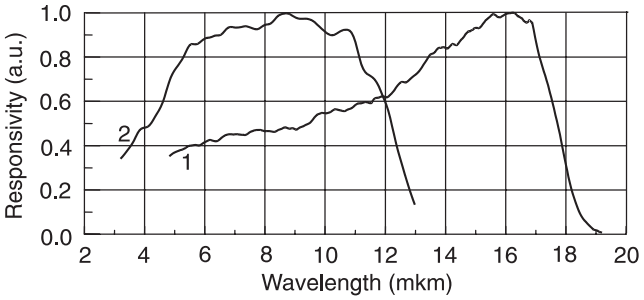

Fig. 8. Spectral dependencies of very long wavelength photoconductor (curve 1) and typical photodiode (curve 2) of FPA (256×256, 40 μm spacing). Operating temperature 77 K.

Linear photoconductors (up to 128 element) operating at 8–12 were produced by the technology of Moscow factory "Alpha" [29,30]. Volt-current (V-I) characteristics are ohmic with bias up to 0.8 V. High uniformity detectivity and photoresponse of photosensitive elements was $(4–6)\times10^{10}$ cmHz$^{1/2}$/W and $(6–9)\times10^{4}$ V/W respectively with the maximum response at 10.5 μm. The testing of influence of vibrations, shocks, elevated temperature (60°C) showed the absence of changing detectors parameters which remained at the same level after 12-month operation.

4.2. Photodiodes

The technology of fabrication of photovoltaic focal plane arrays was developed and the main steps of it are the following:

- covering of chemically cleaning MCT surface by photoresist and opening windows,
- ion implantation by B^+,
- low temperature deposition of SiO_2 and Si_3N_4 dielectric coating,
- opening windows in dielectric coating,
- indium deposition for contacts,
- formation of indium bumps.

The specification of 128×128 FPA's which operated at different wavelengths and temperatures is presented in Table 2 [31].

Table 2. FPAs specification

Cut-off wavelength (μm)	6.0	8.7	12.8	4.6
Cell size (μm)	25×25			
Array pitch (μm)	50×50			
Operating temperature (K)	79–80			210–215
Frame rate (Hz)	50			
Integration time (μs)	930	130		450
NEDT (K) (backgr. temp. 295 K)	0.019	0.025	0.029	0.45
FOV, 2Θ (deg)	40	40		70

The V-I characteristics, differential resistance, spectral response, noise equivalent temperature differences (NETD) were measured by using a multiplexer with arbitrary access to elements in combination with current-voltage transformer. The FPA's were installed in cryostat and cooled down to liquid nitrogen or elevated temperatures. The angular aperture was restricted to a cooled diaphragm.

In Fig. 9(a,b), typical diode V-I characteristics and differential resistance are shown for 128×128 FPA with wavelength cut-off λ_c = 6 μm at 78 K. Reverse current is practically constant up to the bias voltage –0.4 V and slightly decreasing when the bias voltage increases up to –1 V. The R_0A products are 6×10^3 Ω cm^2 and in maximum 2.5×10^5 Ω cm^2.

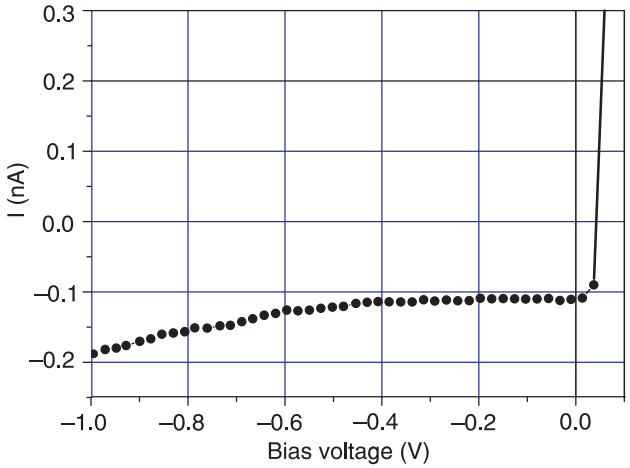

Fig. 9(a). Typical diodes V-I characteristics (FPA, λ_c = 6.0 m).

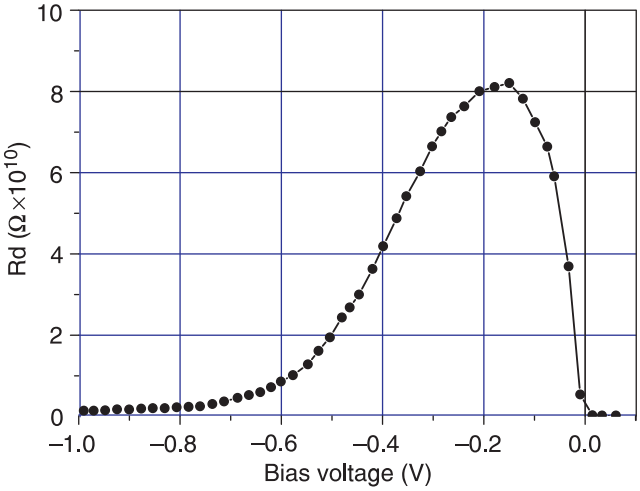

Fig. 9(b). Typical diodes differential resistance (FPA, λ_c = 6.0 m).

In Figs. 10(a) and 10(b), the V-I characteristics and differential resistance are shown for FPA with wavelength cut-off 8.7 μm at 78 K. Reverse current monotonously weakly decrease when the bias voltage increases up to –0.5 V. The R_0A product are 22 Ω cm^2 and in maximum 3.6×10^2 Ω cm^2. It is necessary to remark that the serial resistance for diode is less than 10 Ω.

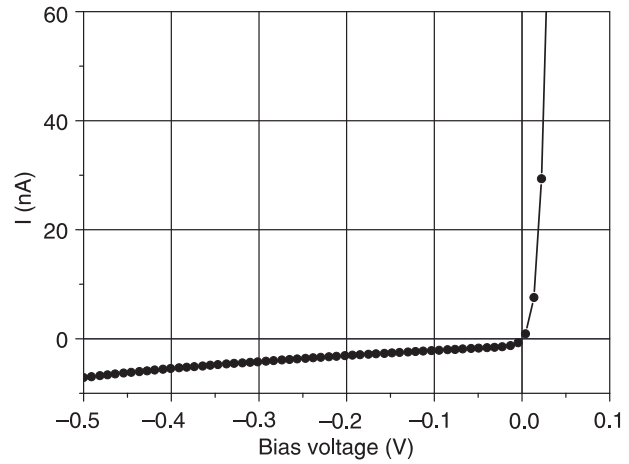

Fig. 10(a). Typical diodes dark V-I characteristics (FPA, λ_c = 8.7 μm).

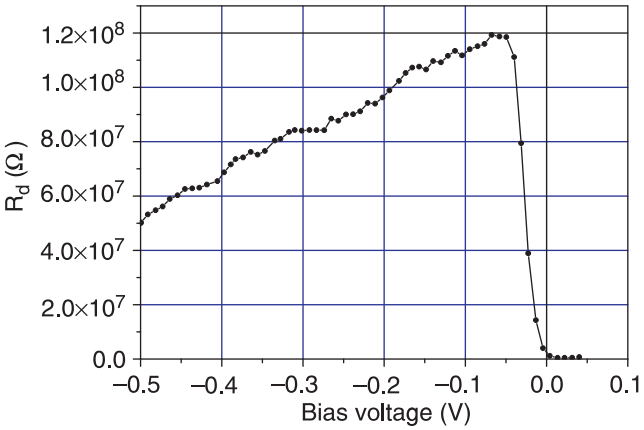

Fig. 10(b). Typical diodes differential resistance (FPA, λ_c = 8.7 μm).

In Figs. 11(a) and (b), the histograms of NETD's show the high uniformity of temperatures difference of FPA's which is equal to 19.3 mK for λ_c = 6.0 μm and 24.8 mK for λ_c = 8.7 μm.

Figure 12 demonstrates thermal images of a man leaning on a car (a) and man's face and hand with blood veins (b).

4.3. Simulation of diode characteristics

The novel structures with graded MCT composition throughout the thickness grown by MBE allow to obtain additional advantages for increasing parameters of photosensitive diodes, such as: the serial resistance R_s decreasing and R_0A product and detectivity D^* increasing.

The calculations [32] were performed within the context of a one-dimensional diffusion-drift model including the Poisson and continuity equations for electrons and holes, which take into account carriers recombination R (Auger, Shockley-Read, and radiative mechanisms [33]) and photogeneration G and the built-in field arising because of the dependence of the band structure parameters on the coordinate

$$\Delta\varphi = -\frac{q}{\varepsilon_s\varepsilon_0}(p - n - N_A^- + N_D^+), \tag{4}$$

$$\frac{1}{q}\Delta\vec{j}_n = -(G - R), \tag{5}$$

$$\frac{1}{q}\Delta\vec{j}_p = G - R, \tag{6}$$

$$G(y) = \alpha(y)\Phi\exp\left(-\int_0^y a(y')dy'\right), \tag{7}$$

where Φ is the flux of radiation and α is the adsorption coefficient [34]. Electron and hole currents are expressed by

$$\vec{j}_n = n\mu_n\Delta E_{Fn}, \quad \vec{j}_p = p\mu_p\Delta E_{Fp}. \tag{8}$$

taking into account Fermi quasilevels E_{Fn} and E_{Fp} [35].

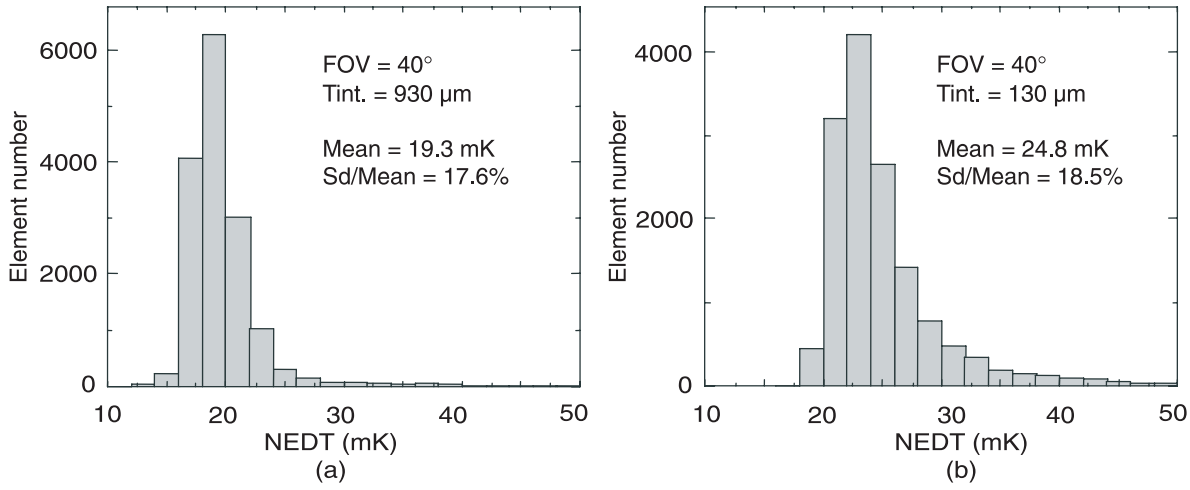

Fig. 11. (a) NEDT of 128×128 FPA, λ_c = 6.0 μm, (b) NEDT of 128×128 FPA, λ_c = 8,7 μm.

(a) (b)

Fig. 12. (a) Thermal image of man and car (FPA, λ_c = 6.0 μm), (b) Thermal image of face and hand with blood veins.

The electron and hole concentration and Fermi quasilevels E_{Fn} and E_{Fp} are given by

$$n = n_i \exp\left(\frac{E_{Fn} - E_i}{k_B T}\right), \quad p = n_i \exp\left(\frac{E_i - E_{Fp}}{k_B T}\right), \quad (9)$$

where n_i is the intrinsic carrier concentration and E_i is the Fermi level into intrinsic semiconductor and is expressed by

$$E_i = -q\varphi - \chi - \frac{E_g}{2} - \frac{3}{4} k_B T \ln \frac{m_n}{m_p}, \quad (10)$$

where χ is the electron affinity.

The series resistance R_s is important in fabricating high frequency photodetectors and together with junction capacitance it determines the maximum operating frequency. For heterodyne diode, the high value R_s leads to significant change of operating point. The R_s parameter is important for multielement photovoltaic linear and two-dimensional arrays. In this case, series resistance to the base contact has a different value for central and peripheral elements. The high values of R_s lead to high values of the total current for multielement FPA's at which photodiodes operating point will change. Practically, this is equivalent to increase in cross talking and can give additional contribution to FPA noise. When n-p junctions are formed on the basis of p-type MCT epitaxial layers with constant composition, the R_s value up to a few tens kilohm is typical.

R_s value can be decreased by growing in p-type MCT film a narrow gap layer in base contact region. In general, the presence of narrowgap layers leads to the quantum efficiency decrease. We performed a numerical simulation of n-p junction parameters in order to determine MCT composition profile allowing to decrease the R_s and to maintain the quantum efficiency value simultaneously. It was found that forming a narrowgap layer in the MCT film at the interface with the buffer layer and subsequent wide gap layer leads to decrease in R_s practically without decrease in quantum efficiency [see Fig. 4(b)]. The experimental data were in agreement with calculation results. Really, we fabricate diodes on the basis of MCT HS's MBE with widegap layer (type 1), narrowgap (type 2) layer at interface MCT film/buffer layer and with narrowgap and subsequent widegap layer (type 3). Low R_s (a few ohm) was obtained for diodes based on MCT HS's of types 2 and 3, and high R_s values (hundreds of ohm) were obtained for type 1. The spectral sensitivity of diodes of type 3 was close to the theoretical value. At the same time diodes of type 2 had spectral sensitivity value significantly lower than the calculated one, particularly for a longer spectrum range.

The heterodyne diodes of type 3 with 300 μm in diameter and λ_c = 12.1 μm was fabricated. At direct detection the threshold power of the photodiode at 10.6 μm wavelength is 5.9×10^{-14} W/Hz$^{1/2}$ in mode without background radiation and 3.7×10^{-13} W/Hz$^{1/2}$ with background (2θ = 76°, T = 195 K). The measurements were performed at 1 kHz frequency. The diodes were tested in heterodyne regime. The measurements were carried out on an installation at intermediate frequency 11.3 MHz using CO_2 laser (λ = 10.6 μm) at heterodyne power from 0.1 up to 1 mW. We put our diode instead of an industrial photodetector FUO144 («Tsukat») with threshold power 5×10^{-20} W/Hz at pumping with 0.8 mW. We measured analogous threshold power at pumping power 0.2 mW.

We performed the calculation of such diodes characteristics as detectivity D^* [$D^* = R_\lambda (A\Delta f/I_n)^{1/2}$], maximum sensitivity R_λ ($R_\lambda = \eta q/hc$) and R_0A product [$R_0A = A(dI/dV)^{-1}$] at different locations of p-n junction in MCT heteroepitaxial structures with active layer 10 μm in thickness and wide gap thickness 1 μm at film surface. Here A is the

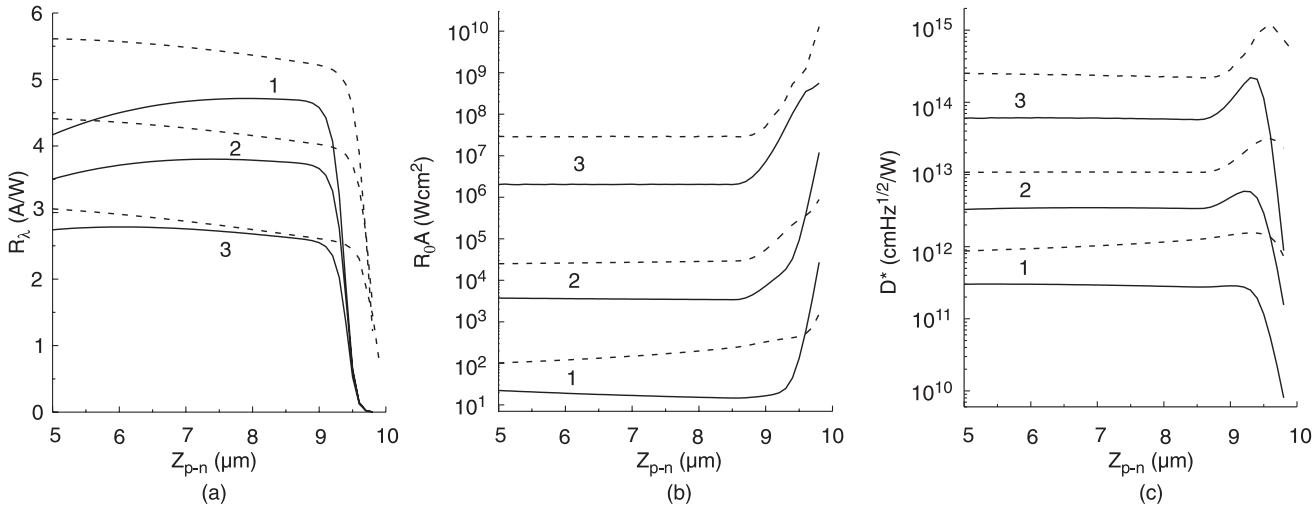

Fig. 13. (a) The dependence of R_λ on p-n junction location. (b) The dependence of R_0A products on p-n junction location. (c) The dependence of D^* on p-n junction location.

diodes area, Δf is the frequency band, I_n is the noise current, η is the quantum efficiency, and q is the electron charge.

MCT composition in active layer was X_{CdTe} = 0.22, 0.25, and 0.3. The n-p junction location varied from the middle part of the diode to its surface. The carrier concentration value is 10^{16} cm^{-3} in p-type region and 10^{17}cm^{-3} in n-type one. The n-p junction is assumed to be abrupt. The structure was illuminated from the substrate side.

The calculation results [36] for R_λ, R_0A and D^* dependencies on the position of n on p (n-p) junction ($Z_{p\text{-}n}$) for different X_{CdTe} are presented in Figs. 13(a), 13(b) and 13(c) (solid lines). Independently on X_{CdTe} in the active layer a sharp decrease in R_λ and increase in R_0A product was observed when n-p junction location is close to the surface region (~1 μm). However, increase in R_0A product takes place faster than decreasing R_λ. So, this leads to appearance of maximum in D^* at 0.7–0.8 μm from the film surface. The D^* maximum is 3.5 times higher than D^* in case of n-p junction location in the active layer with constant X_{CdTe} = 0.3. It is interesting to note that with significant R_0A increase there is observed a relatively low decrease in D^* value. Thus, for X_{CdTe} = 0.22, at n-p junction location at 0.4 μm from the surface, the R_0A product is 30 times higher than for n-p junction location in active layer with D^* being only in 5.5 times lower. For MCT HS's structures with X_{CdTe} = 0.25 R_0A value increases 110 times with D^* being 2.5 times lower.

Analogous characteristics of R_λ, R_0A and D^* were calculated for p on n (p-n) junction with doping level in n-type 10^{15} cm^{-3} and in *p*-type 10^{16} cm^{-3} [Figs. 11(a), 11(b) and 11(c) – dashed lines]. Some different features were observed for p-n structures. The change of R_0A product varies significantly less at the p-n junction shift to the graded gap region than for n-p structures. Furthermore, at X_{CdTe} = 0.22 slow increase in R_0A begins even in the active layer. For all X_{CdTe} the R_λ value in p-n structures increases steadily with the p-n junction shift to the surface and then decreases dramatically in the graded gap region. The D^* value increases when p-n junction is shifted to the surface and achieves maximum in the graded gap region. The subsequent D^* decrease for p-on-n structures is weaker than for n-on-p ones.

Thus, numerical calculations demonstrate the possibility of improving the characteristics of the photodiodes based on MCT graded gap layers when the n-p junction is formed in the graded gap region. The p-n photodiodes offer some advantages over the n-p diodes.

5. Conclusions

The basic and specific physical and chemical features at MCT heterostructure growth on GaAs substrates and defects formation mechanisms were discussed. The ways of decreasing defects to minimal values and growing MCT films of high quality on GaAs substrate were determined.

A new generation of industrially oriented ultra high vacuum set for MBE growth of MCT HS's with *in situ* ellipso-metric control and automated control of technological processes was developed and produced.

The industrially oriented technology of MCT HS's MBE growth on 2'' (013)GaAs substrate for multielement photodiodes and photoconductors arrays was developed.

Single, linear and focal plane arrays of high quality were fabricated on the basis of MCT heterostructures on GaAs. Calculation and experimental results of detector characteristics revealed improving series resistance in diodes fabricating on the basis of MCT films with narrowgap layer. The increase in detectivity was found at optimal p-n junction location at graded widegap layer near the MCT film surface.

Acknowledgements

Authors would like to acknowledge L.D. Burdina, O.I. Malyshev for the help in growing MCT HS, A.P. Antsiferov for designing elements of MBE set, T.I. Zakhariyash for fabricating FPA and photoconductive elements, E.V. Susov and G.V. Chekanova for fabricating linear photoconductors.

References

1. J.P. Zanatta, P. Ferret, G. Theret, A. Million, M. Volny, J.P. Chamonal, and G. Destefanis, "Heteroepitaxy of HgCdTe (211)B on Ge substrates by molecular beam epitaxy for infrared detectors", *J. Electron. Mat.* **27**, 542 (1998).
2. S.D. Chen, L. Lin, X.Z. He, Z.Y. Xu, C.P. Luo, and J.Z. Xu, "High-resolution photoluminescence studies of (211) CdTe grown on (211) GaAs substrate", *J. Cryst. Growth* **140**, 287 (1994).
3. Yu.G. Sidorov, S.A. Dvoretsky, V.S. Varavin, N.N. Mikhailov, M.V. Yakushev, and I.V. Sabinina, "Molecular beam epitaxy of mercury cadmium telluride solid solution on alternative substrate", *Semiconductors* **35**, 1092 (2001).
4. K. Kokie, T. Tanaka, S. Li, and M. Yano, "High-quality CdTe growth in the (100)-orientation on (100) GaAs substrate by molecular beam epitaxy", *J. Cryst. Growth* **227–228**, 671 (2001).
5. T.J. de Lyon, D. Rajavel, S.M. Johnson, and C.A. Cockrum, "Molecular-beam epitaxial growth of CdTe(112) on Si(112) substrates", *Appl. Phys. Lett.* **66**, 2129 (1995).
6. M. Kawano, A. Ajisawa, N. Oda, M. Nagashima, and H. Wada, "HgCdTe and CdTe(1 1 3)B growth on Si(112)5° off by molecular beam epitaxy", *Appl. Phys. Lett.* **69**, 2876 (1996).
7. D.J. Smith, S.C. Y. Tsen, D. Chandrasekhar, P.A. Crozier, S. Rujirawat, G. Brill, Y.P. Chen, R. Sporken, and S Sivananthan, "Growth and characterization of CdTe/Si heterostructures – effect of substrate orientation", *Mat. Sci&Eng.* **B77**, 93 (2000).
8. R.E DeWames, D.D. Edwall, M. Zandian, L.O. Bubulac, J.G. Pasko, W.E. Tennant, J.M. Arias, and A. D'Souza. "Dark current generating mechanism in shot wavelength infrared photovoltaic detectors", *J. Electron. Mat.* **27**, 772 (1998).
9. A. D'Souza, J Bajaj, R.E DeWames, D.D. Edwall, P.S. Wijewarnasurija, and N. Nayar, "MWIR DLPH HgCdTe perfomance dependence on substrate material", *J. Electron. Mat.* **27**, 727 (1998).
10. V.V. Vasiliev, D.G. Esaev, T.I. Zakhariyash, A.G. Klimenko, A.I. Kozlov, I.V. Marchishin, V.N. Ovsyuk, N.Kh. Talipov, Yu.G. Sidorov, and S.A. Dvoretsky, "128×128 hybrid FPA using MBE HgCdTe films on GaAs substrates. Optoelectronics", *Instrument & Data Process.* **N4**, 22 (1998).
11. A. D'Souza, L.C. Dawson, C. Staller, P.S. Wijewarnasurija, R.E DeWames, W.V. MacLevige, J.M. Arias, D. Edwall, and G. Hilderbrandt. "Large VLWIR HgCdTe photovoltaic detectors", *J. Electr. Mat.* **29**, 630 (2000).
12. S.M. Johnson, J.L. Johnson, W.J. Hamilton, D.B. Leonard, T.A. Strand, E.A. Patten, J.M. Peterson, J.H. Durham, V.K. Randall, T.J. deLyon, J.E. Jensen, and M.D. Gorwitz, "HgCdZnTe quaternary materials for lattice-matched two-colour detectors", *J. Electron. Mater.* **29**, 680 (2000).
13. J.M. Arias, R.E. DeWames, S.H. Shin, J.G. Pasko, J.S. Chen, and E.R. Gerther, "Infrared diodes fabricated with HgCdTe grown by molecular beam epitaxy on GaAs substrates", *Appl. Phys. Lett.* **54**, 1025 (1989).
14. K. Jóźwikowski, and A. Rogalski, "Effect of dislocations on performance of LWIR HgCdTe photodiodes", *J. Electron. Mater.* **29**, 736 (2000).
15. J.M. Arias, M. Zandian, S.H. Shin, W.V. McLevige, J.G. Pasko, and R.E. DeWames, "Dislocation density reduction by thermal annealing of HgCdTe epilayers grown by molecular beam epitaxy on GaAs substrates", *J. Vac. Sci. Technol.* **B9**, 1646 (1991).
16. V.M. Osadchy, A.O. Suslyakov, V.V. Vasiliev, S.A Dvoretsky, "Effective carriers lifetime in varizone structures on CdHgTe", *Fizika Technika Poluprovodnikov*, **33**, 293 (1999). (in Russian).
17. Y. Nemirovsky, R. Fastow, M. Meyassed, and A. Unikovsky., "Trapping effects in HgCdTe", *J. Vac. Sci. Technol.* **B9**, 1829 (1991).
18. M. Tanaka, K. Ozaki, N. Nishino, H. Be, and Y Miyamoto, "Electrical properties of HgCdTe doped with silver using an $AgNO_3$ solution", *J. Mater. Sci.* **27**, 579 (1998).
19. J.M. Arias, "Growth of HgCdTe by molecular beam epitaxy" in *Properties of Narrow Gap Cadmium-based Compounds*, edited by P. Capper, p. 30, INSPEC, Institution of Electrical Engineers, London, United Kindom, 1994.
20. Yu.G. Sidorov and E.M. Trukhanov, "About possibility of formation of amorphous phase at heterostructure formation with large lattice mismatch", *Poverhnost* **N6**, 106, (1992). (in Russian).
21. S.A. Dvoretsky, V.P. Zubkov, V.V. Kalinin, V.D. Kuzmin, and Yu.G. Sidorov, "Investigation of initial stage at molecular beam epitaxy of CdTe on GaAs(100)", *Poverhnost* **N9**, 45 (1991). (in Russian).
22. Yu.G. Sidorov, S.A. Dvoretsky, M.V. Yakushev, N.N. Mikhailov, V.S. Varavin, and V.I. Liberman, "Peculiarities of the MBE growth physics and technology of narrow-gap II-VI compounds", *Thin Solid Films* **306**, 253 (1997). (in Russian).
23. E.V. Spesivtsev and S.V. Rykhlitski, "Ellipsometer", Inventor's certificate RF No. 16314 of 20.12.2000. (in Russian)
24. Yu.G Sidorov, S.A. Dvoretsky, N.N. Mikhailov, M.V. Yakushev, V.S. Varavin, and A.P. Antsiferov, "Molecular beam epitaxy of narrow gap compositions $Cd_xHg_{1-x}Te$. Equipment and technology", *Optichesky Zhournal* **67**, 39 (2000). (in Russian).
25. V.S. Varavin, S.A. Dvoretsky, N.N. Mikhailov, and Yu.G. Sidorov, "Donor defects in HgCdTe epitaxial layers grown by molecular beam epitaxy", *Avtometriya* **N3**, 9 (2001). (in Russian).
26. V.S. Varavin, S.A. Dvoretsky, V.I. Liberman, N.N. Mikhailov, and Yu.G. Sidorov, "Molecular beam epitaxy of high quality HgCdTe films with control of composition distribution", *J. Cryst. Growth* **159**, 1161 (1996).
27. A.V. Voitsekhovsky, Yu.A. Denisov, A.P. Kokhanenko, V.S. Varavin, S.A. Dvoretsky, N.N. Mikhailov, Yu.G. Sidorov, and M.V. Yakushev. "Peculiarities of spectral and recombination characteristics of MBE structures on CdHgTe", *Avtometriya* **N4**, 47 (1998). (in Russian).

28. Yu.G. Sidorov, S.A. Dvoretsky, N.N. Mikhailov, M.V. Yakushev, V.S. Varavin, V.V. Vasiliev, A.O. Suslyakov, and V.N. Ovsyuk, "MCT heterostructures designing and growing by MBE for IR devices", *Prikladnaya Fizika* **N5**, 54 (2000).
29. E.V. Susov, Yu.G. Sidorov, V.N. Severtsev, A.A. Komov, G.V. Chekanova, S.A. Dvoretsky, V.S. Varavin, N.N. Mikhailov, and L.I. D'yakonov, "Multielement photoresistor with HgCdTe heterostructures", *Avtometriya* **N4**, 40 (1996). (in Russian).
30. E.V. Susov, V.S. Varavin, S.A. Dvoretsky, N.N. Mikhailov, and G.V. Chekanova, "128-element cooled IR devices based on CdHgTe heteroepitaxial structures", *Instrument & Data Process* **N4**, 17 (1998).
31. V.V. Vasiliev, S.A. Dvoretsky, D.G. Esaev, T.I. Zakhariyash, A.G. Klimenko, A.I. Kozlov, I.V. Marchishin, V.N. Ovsyuk, N.Kh. Talipov, Yu.G. Sidorov, and A.O. Suslyakov, "Photodetectors on the basis of CdHgTe layers grown by molecular beam epitaxy", *Avtometriya* **N3**, 4 (2000). (in Russian).
32. V.S. Varavin, V.V. Vasiliev, T.I. Zakhariyash, S.A. Dvoretsky, N.N. Mikhailov, V.N. Ovsyuk, V.M. Osadchy, Yu.G. Sidorov, and A.O. Suslyakov, "Phototdiodes with low serial resistance with graded band gap HgCdTe epitaxial films", *Optichesky Zhournal* **66**, 69 (1999). (in Russian).
33. A. Rogalski and J. Piotrowski, "Intrinsic infrared detectors", *Prog. Quant. Electron.* **12**, 87 (1988).
34. W.W. Anderson, "Absorption constant of $Pb_{1-x}Sn_xTe$ and $Hg_{1-x}Cd_xTe$ alloys", *Infrared Phys.* **20**, 363 (1980).
35. K.M. Van Vlliet and A.H. Marshak, "The Shockley-like equation for the carrier densities and current flow in materials with a nonuniform composition", *Solid State Electron.* **23**, 49 (1980).
36. V.N. Ovsyuk, V.V. Vasiliev, N.Kh. Talipov, L.N. Romashko, A.I. Kozlov, and I.V. Marchishin, "Photodetectors on basis of HgCdTe films grown by molecular beam epitaxy", in *Matrichnie Fotopriemnie Ustroistva Infrakrasnogo Diapasona*, edited by S.P. Sinitsa, p. 179, Nauka, Novosibirsk, 2001.

Forthcoming conferences

Readers are invited to send the Executive Editor details of conference to be announced

13–18 July
Chemistry of Electronic Materials, New London, CT, USA
Organic devices, novel deposition techniques, and semiconductor processing will be covered.

20–25 July
High Temperature Corrosion, New London, NH, USA
Internal oxidation, stress development, and ways of tailoring oxide properties will be discussed.

20–25 July
Biomaterials: Biocompatibility/Tissue Engineering, Plymouth, NH, USA
Topics include scaffold architecture, biohybrid materials, and tissue biomechanics.

27–1 August
Fuel Cells, Bristol, RI, USA
Focusing on new cell materials, next generation fuel cells, and fundamental understanding of fuel cells.
Tel: +1 401 7834011
Fax: +1 401 783 7644
E-mail: grc@grc.org
URL: www.grc.org

14–16 August
Faraday Discussion 125 on Nanoparticle Assemblies, Liverpool, UK
Discussion of the relationship between nanoparticle properties and self-organization at the nanoscale. Tel: +44 (0)20 7437 8656
Fax: +44(0)20 7734 1227
E-mail: hallc@rsc.org
URL: www.rsc.org

14–16 August
Fatigue Damage of Materials 2003, Toronto, Canada
Focusing on testing and analysis methods, failure mechanisms, high and low cycle fatigue, cyclic elastoplastic behavior, materials, and structures.
Tel: +44 (0)238 029 3223
Fax: +44 (0)238 029 2853
E-mail: gmckeogh@wessex.ac.uk
URL: www.wessex.ac.uk

14–18 August
ICCM-14: 14th International Conference on Composite Materials, San Diego, CA, USA
Conference theme and scope will emphasize bridging the gap between academia and industry.
Tel: +1 313 271 1500
Fax: +1 313425 3401
E-mail: service@sme.org
URL: www.sme.org/iccm14

14–18 August
SEMICON West, San Francisco and San Jose, CA, USA
New for this year: programs on MEMS, the semiconductor roadmap, and a partnership with SPIE.
Tel: +1 408943 7009
E-mail: semiexpositions@semi.org
URL: www.semi.org

28–30 August
ICSAM 2003: 8th International Conference on Superplasticity in Advanced Materials, Oxford, UK
Topics will include diffusion bonding, microstructure-macroproperty relationships, presses and tooling, product design, new alloys, and applications.
Fax: +44 (0)1865 273783
E-mail: icsam2003@materials.ox.ac.uk
URL: www.materials.ox.ac.uk/icsam2003

27–1 August
ICM 2003: International Conference on Magnetism, Rome, Italy
Sessions include hard and soft magnetic materials, spintronics, molecular and nanoscopic magnetism, techniques and applications.
Tel: +39 (0)6 9067 2285
Fax: +39 (0)6 9067 2470
E-mail: icm2003@mlib.cnr.it
URL: www.icm2003.mlib.cnr.it

29–1 August
MC6: 6th International Conference on Materials Chemistry, Sheffield, UK
Conference themes are solid state chemistry, polymer chemistry, and liquid crystals.
Tel: +44 (0)20 7437 8656
Fax: +44 (0)20 7734 1227
E-mail: conferences@rsc.org
URL: www.rsc.org

3–7 August
ICE 2003: International Conference on Electroceramics, Cambridge, MA, USA
Emerging R&D issues and the latest technology, as well as traditional topics, will be addressed.
Contact: Elisabeth Anderson
E-mail: ice-2003@mit.edu
URL: http://ice-2003.mit.edu

3–7 August
Microscopy and Microanalysis 2003, San Antonio, TX, USA
Program will cover alt aspects of microscopy and microanalysis; nanotechnology will be emphasized.
Contact: David Piston
Tel: +1 6153436440
Fax: +1 615 343 1103
E-mail: dave.piston@vanderbilt.edu
URL: www.microscopy.org

3–8 August
48th SPIE Annual Meeting, San Diego, CA, USA
Expo and conference on optical science, including organic photonics, electronics, and nanotechnology.
Tel: +1 3606763290
Fax: +1 360647 144S
E-mail: spie@spie.org
URL: www.spie.org

4–8 August
Denver X-Ray Conference, Denver, CO, USA
Special sessions will cover new developments in X-ray diffraction and fluorescence.
Contact: Denise Flaherty
Tel: +1 6103259814
Fax: +1 610325 9823
E-mail: flaherty@iicdd.com
URL: www.dxcicdd.com

4–8 August
Spintech II: 2*nd* International Conference on Semiconductor Spintronics and Quantum Information Technology, Brugge, Belgium
Symposium will focus on spin transport, as well as applications in nanoelectronics and computing.
Tel: +1 703 7974570
E-mail: spintech2@sainc.com
URL: www.sainc.com/spintech2

